
Article:
Watson, M. and Marshall, M.B. (2018) Wear mechanisms at the blade tip seal interface. Wear, 404-05. pp. 176-193. ISSN 0043-1648

https://doi.org/10.1016/j.wear.2018.03.009

Wear 404–405 (2018) 176–193

Contents lists available at ScienceDirect

Wear

journal homepage: www.elsevier.com/locate/wear

Wear mechanisms at the blade tip seal interface

Michael Watson*, Matthew Marshall

University of Sheffield, Sir Frederick Mappin Building, Mappin St Sheffield, S1 3JD UK

ARTICLE INFO

Keywords:
Abradable
High speed wear testing
Gas turbine sealing

ABSTRACT

Abradable seals are used at the interface between blade tips and compressor casings in modern gas turbine engines. These materials wear in preference to the blade tips leaving a track which perfectly fits the blades, thus improving sealing at the blade tip an increasing both efficiency and stall margin of the compressor.

The wear mechanisms occurring at this interface have been characterised for two common abradable materials. Changes to these mechanisms with blade speed, incursion rate and abradable hardness have been investigated and described statistically. The wear mechanisms proposed in this work and previously suggested have been used as the foundation for linear models which have been fitted to the results. These models have been used to test the quality of the mechanisms and indicate which processes are poorly understood.

The models were well correlated to results for forces with normally distributed residuals indicating rubbing force systems are well represented by the proposed mechanisms. Temperature and blade length change results were less well correlated indicating these processes are more poorly understood. This work shows that simple linear models based on a mechanistic understanding of underlying processes can be used for describing forces.

1. Introduction

Abradable materials are used in gas turbine engines to maintain seals at the compressor blade tips. An abradable lining on the casing wears in preference to the blades maintaining the minimum possible gap between the blades and the casing and reducing tip leakage flows and improving the efficiency and stall margin of the compressor [1].

In the low pressure compressor AlSi based abradables are used against titanium blades [2]. In the high pressure compressor temperatures are prohibitively high for both titanium blades and the AlSi alloy used in these abradables [3]. For these stages Inconel 718 blades are run against a NiCrAl bentonite abradable [4].

Research on these rubbing systems is largely carried out on scaled test rigs which aim to recreate the conditions present in service. Research on the AlSi polyester abradable [5] has consistently shown adhesion from the abradable to the blade tip with some blade wear at low incursion rates as seen in service. Cutting behaviour is observed at high incursion rates, similar to turning or milling of the abradable.

However each of the previous studies on this abradable has only considered a single spray batch. Recent work in the field by Fois et al. [6] has shown large effects resulting from changes in the spraying process within the typical range. These result in differences in the hardness and thermal properties of the abradable [7]. No studies have been identified that investigate the effect of these changes on the AlSi Polyester abradable.

Research on the NiCrAl bentonite vs Inconel 718 system has shown the abradable wears with low forces at very low incursion rates leaving a rough dull surface [8,9]. At higher incursion rates blade wear is seen with compaction of the surface leading to very high forces. Again both of the studies on this system have focused on a single spray batch.

Typically studies in this field consist of a relatively small number of experimental tests on a single spray batch of abradable. The aim of these studies is to map the behaviour of the abradable under different incursion conditions so that optimal conditions can be identified or particularly damaging mechanisms avoided in service [2,10]. The behaviour is determined by post mortem examination of the worn samples.

While this approach allows the wear mechanisms to be quickly characterised, conclusions drawn on the effect of blade speed and incursion rate based on very small numbers of tests with highly random abradable samples from a single spray batch should be treated with caution. In addition as there are very few tests completed as part of

* Corresponding author.
E-mail addresses: mea08mw@googlemail.com (M. Watson), m.b.marshall@sheffield.ac.uk (M. Marshall).

https://doi.org/10.1016/j.wear.2018.03.009
Received 27 June 2017; Received in revised form 5 February 2018; Accepted 18 March 2018
Available online 26 March 2018

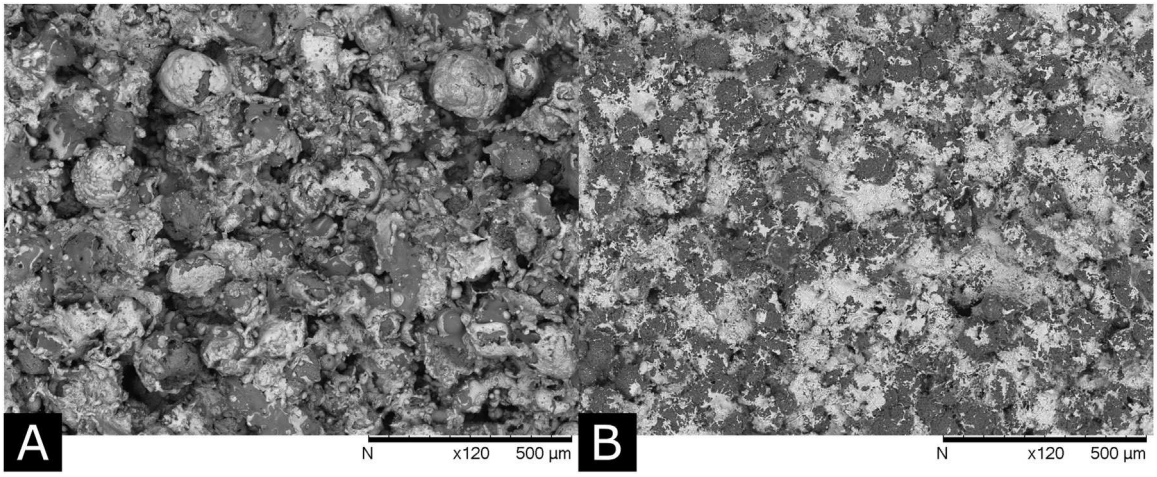

Fig. 1. A and B showing (A) the surface of the NiCrAl bentonite abradable and (B) the surface of the AlSi polyester abradable.

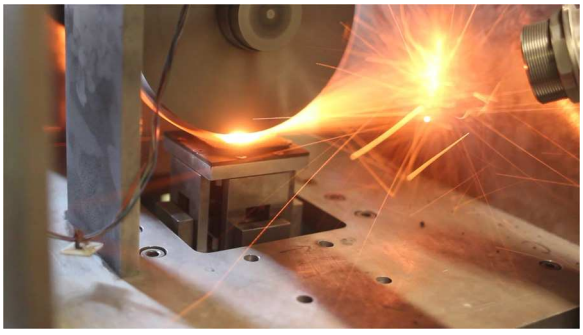

Fig. 2. The experimental rig used for high speed wear testing.

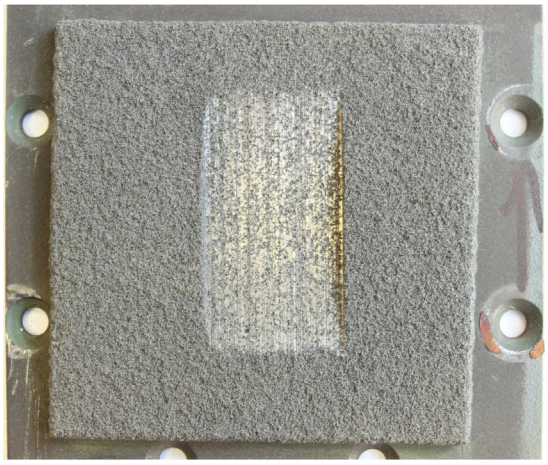

Fig. 3. Showing an example of a worn abradable sample.

these studies the results are typically not statistically tested.

Because of this there is a clear gap in the current understanding of abradables and their performance under different rubbing conditions. This study aims to explore this area of research through testing of large numbers of samples from multiple spray batches. This will allow trends in the results to be analysed in a statistically rigours manner.

In addition, an attempt will be made to apply the growing understanding of these rubbing systems. The mechanisms suggested for each abradable will be used to form the basis of simple models which aim to predict typical mean rubbing conditions after fitting to the results. These mechanisms will also predict different behaviour which can be tested in further studies thus making the proposed mechanisms falsifiable and providing a direction for further studies.

2. Materials and methods

NiCrAl bentonite abradable samples are manufactured by combustion spraying a powder of bentonite particles which have been chemically clad with NiCrAl. This powder is commercially available as Metco 314 ns (Oerlikon Metco Switzerland). The resulting coating has a surface as shown in Fig. 1A. This abradable is exclusively tested against Inconel 718 blades which matches the material combination seen in service in the high pressure compressor. Samples are aged for 100 h at 750 $^{\circ}C$ before testing.

The AlSi polyester abradable samples are made by plasma spraying a power of polyester particles which have been blended with AlSi particles. This powder is commercially available as Metco 601 ns. The resulting coating has a surface as shown in Fig. 1B. These abradable are exclusively tested against Ti (6Al 4 V) blades which matches the material combination seen in service in the low pressure compressor. No heat treatment is carried out before testing.

Tests in this work are performed on a scaled test rig at the University of Sheffield that has been previously described in detail [11] and is shown in Fig. 2. The rig consists of a grinding spindle which holds a 2 mm thick test blade and a dummy blade for balance, the abradable sample is placed on a z axis microscope stage below the blade. Before the test begins the microscope stage is moved so the blade and the abradable surface are just touching. This point is found by binary searching (10 μm accuracy) and compensates for small variations in abradable thickness or blade length.

At the start of the test the abradable is moved back 500 μm and the spindle is rotated to the desired speed. The microscope stage is then used to drive the flat abradable sample into the moving blade at a controlled *incursion rate*. This process produces a intermittent high speed contact between the test blade and the abradable sample. All tests in this work are run at room temperature. An example of a worn abradable sample is shown in Fig. 3.

A stroboscopic imaging system is used to capture images of the

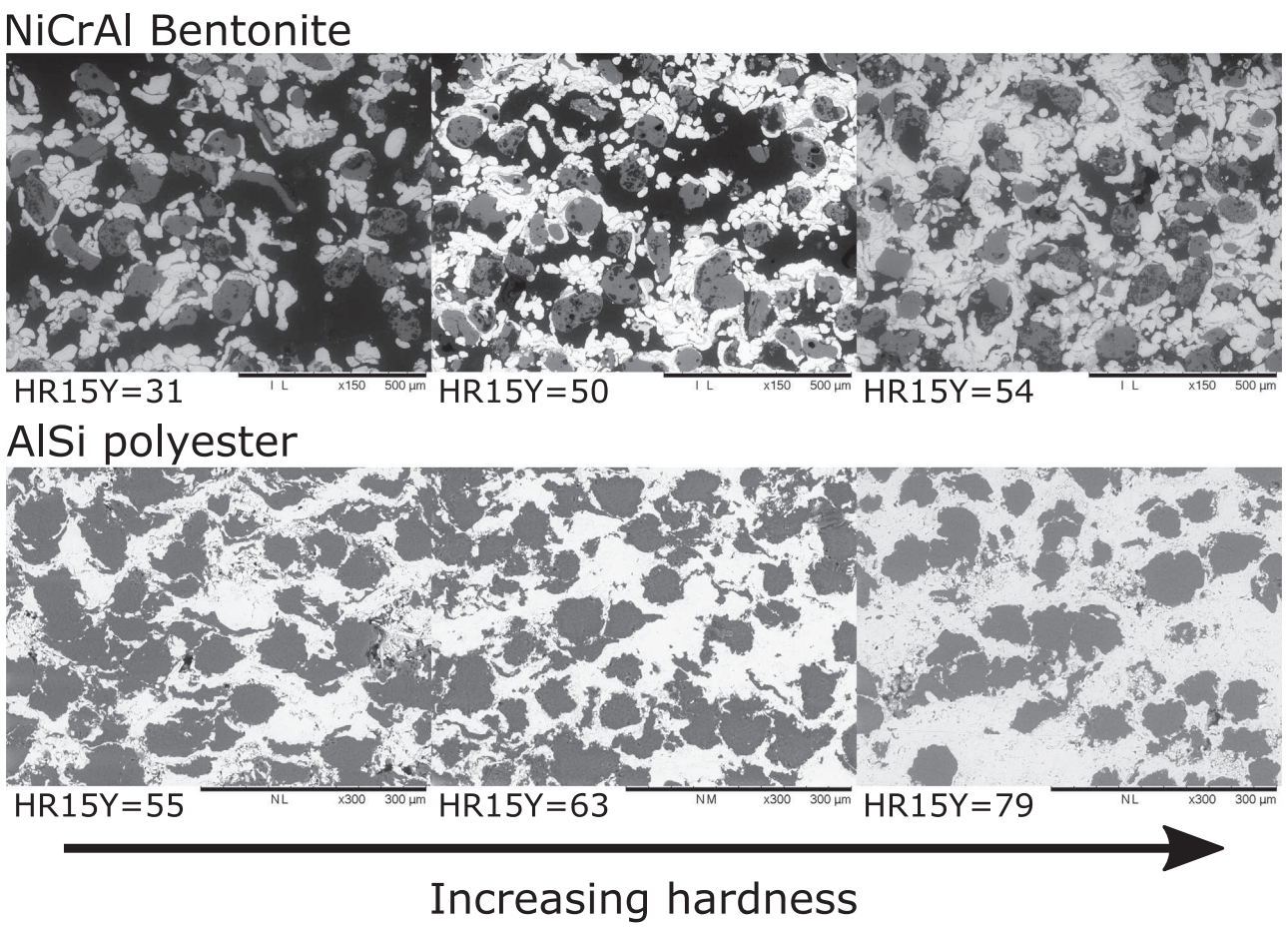

Fig. 4. Cross sections of each of the batches of abradable tested.

blade during the test. This system is described in detail in [11]. The system consists of a camera and an LED which is timed to the rotation of the disc using a light gate and a strobe controller (Gardasoft RT200F-20, Stemmer Imaging Ltd., Surrey, UK). In addition a piezoelectric force transducer (Kistler Instruments Ltd, Hook, (UK), Type 9347C) is placed between the abradable specimen and the microscope stage and a non-contacting infra-red pyrometer (Micro-epsilon, Koenigbacher, Germany) is pointed at the centre of the rubbed section of abradable. These systems are described in detail in [12]. The instrumentation systems allow measurement of the change in blade length from the start of the test, the temperature of the abradable and an indication of the rubbing forces throughout the test.

Both of the abradables have been tested at a range of incursion rates and speeds. Incursion rates of 0.02, 0.2 and 2 $\mu m/pass$ have been chosen. These relate to the running and handling procedure with ten or one blades cutting and an unplanned event such as a bearing crossover respectively. The effect of blade speed has been investigated by testing at 100, 150 and 200 m/s. This upper limit is imposed by the design of the test platform, it should be noted that service conditions see incursions up to 400 m/s blade tip speed, however previous work on this test platform has shown little change in the $100 - 200\ m/s$ range for other AlSi based abradables [10].

Each of these tests has been repeated in triplicate on independent spray batches of abradable. For the AlSi polyester abradable, spray parameters have been controlled to give batches with hardnesses on the industry standard HR15Y scale of 55, 63 and 82 these are referred to as soft, mid and hard batches for the remainder of this work. These relate to the lower end of the specification range, the middle of the range and just above the hardest that would be considered acceptable for service. The combustion spraying process for the NiCrAl bentonite abradable is less well controlled, three batches were sprayed with hardnesses of 31, 50 and 54. Typical images of the microstructure for each batch produced are shown in Fig. 4.

One hundred hardness (HR15Y) and X-ray florescence (XRF) measurements were taken across ten samples for each batch. These were analysed by two way ANOVA's for each abradable. The results showed that significant differences were present between batches however variation between samples from the same batch was not significant. Bonferroni's post tests showed differences between batches were significant for all pairs with the exception of the two hardest batches NiCrAl bentonite abradable. As such, XRF measurements used to identify transfer from the blade to the abradable, will be compared to a control sample from the relevant spray batch.

3. Results

As found by previous work the incursion rate of the blade into the abradable is the driving factor for these rubs. Behaviours observed with the AlSi polyester abradable are also very different to those of the NiCrAl bentonite abradable. As such the results for each abradable are

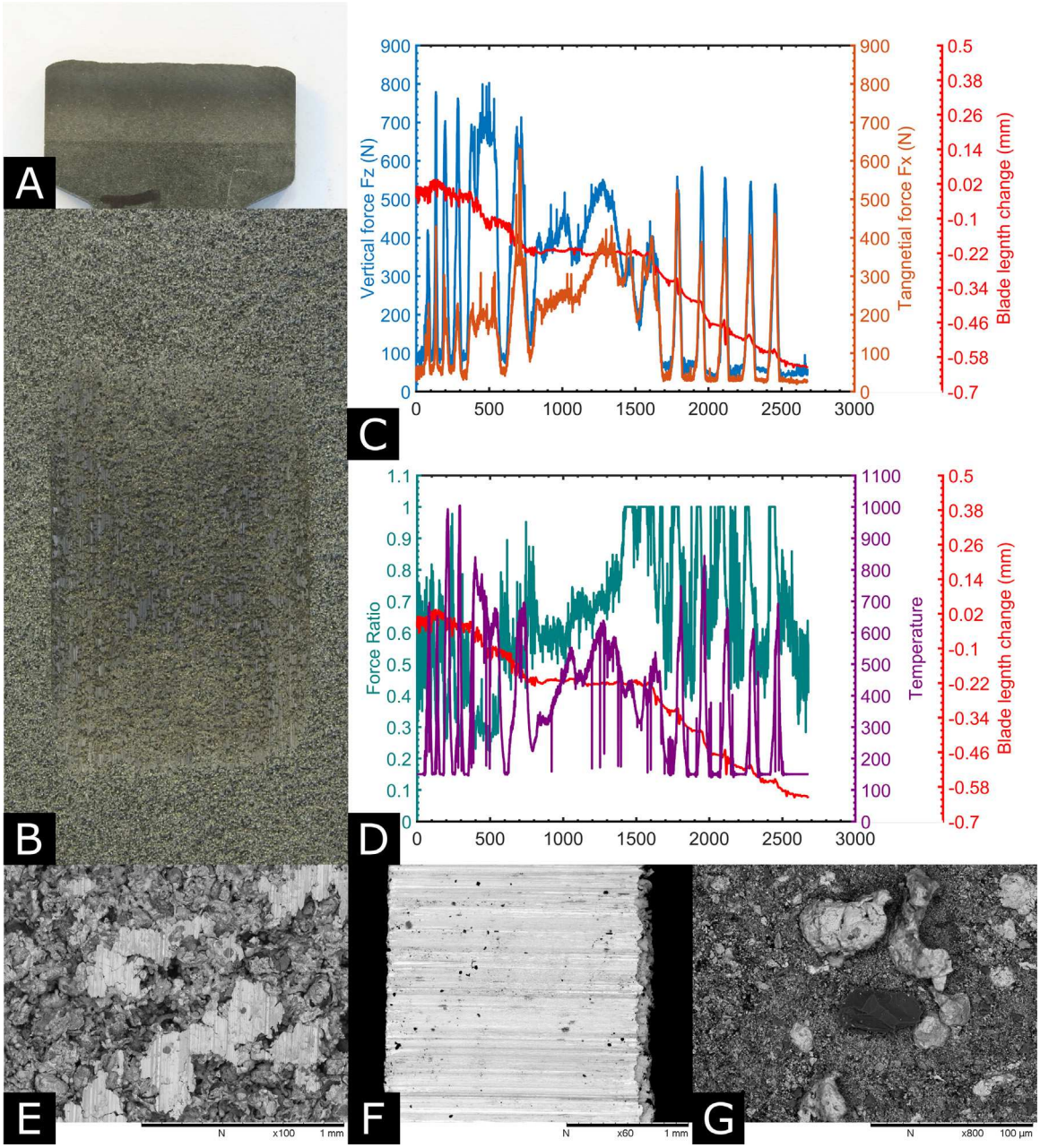

Fig. 5. A–G showing example blade (A) and abradable (B) samples, force and blade length results(C), Temperature and force ratio results (D), and micrographs of the post test abradable surface (E) blade tip (F) and wear debris (G) from tests at 0.02 $\mu m/pass$ against the NiCrAl bentonite abradable.

presented separately and these are further split by the incursion rate used. Each incursion rate has been compared to the other incursion rates by paired *t*-tests with Bonferroni's correction for multiple comparisons, significant differences are highlighted.

3.1. NiCrAl bentonite

3.1.1. 0.02 µm/pass

NiCrAl bentonite abradable samples tested at 0.02 $\mu/pass$ show rough wear tracks with some areas which appear smeared with metal as shown in Fig. 5B. SEM examination of the wear track (Fig. 5E) showed the surface is mostly set back from the arc of contact with the blade with some smeared areas of metal which have contacted the blade.

Blade samples from all tests at all incursion rates show thermal discolouration around the blade tip and a shear lip on the trailing edge of the blade as noted by Taylor et al. [8]. Wear debris gathered from these tests, Fig. 5G consisted of large particles up to 100 μm in diameter.

Force and temperature results from these tests have the form shown in Fig. 5 C and D and previously described by Watson et al. [9]. Cyclic behaviour is observed and thought to be driven by thermal expansion of the rubbing surfaces due to the long period (15 s). This behaviour is

Table 1
Summary of the test data and statistical tests from tests against the NiCrAl bentonite abradable at 0.02 $\mu m/pass$.

H_a	V_b	I_r	F_n (N)		F_t (N)		T_a $(°C)$		Δ_{bl}	XRF
(HR15Y)	(m/s)	$(\mu m/pass)$	Mean	Max	Mean	Max	Mean	Max	mm	(p)
31	100	0.02	570	1150	310	640	470	800	0.038	ns
31	150	0.02	160	300	90	180	220	410	− 0.018	ns
31	200	0.02	190	680	110	380	170	540	− 0.059	ns
50	100	0.02	570	2460	240	1030	270	870	− 1.1	*****
50	150	0.02	260	1490	120	560	320	960	− 1.1	*****
50	200	0.02	270	860	180	550	390	≥ 1000	− 0.62	0.0064
54	100	0.02	850	2040	410	1440	370	790	− 0.25	*****
54	150	0.02	310	1610	210	790	350	910	− 1.0	*****
54	200	0.02	290	800	170	630	360	≥ 1000	− 0.59	*****
p vs 0.2 $\mu m/pass$			0.0023	0.00084	0.0094	ns	0.00078	ns	0.0011	
p vs 2 $\mu m/pass$			0.00043	8.8e − 5	6.6e − 5	0.0013	0.00011	ns	0.048	
Trend with H_a				+ ve		+ ve		+ ve	− ve	
Significance of trend			ns	0.018	ns	0.021	ns	0.019	0.029	
Trend with V_b			− ve	− ve	− ve	− ve				
Significance of trend			0.011	0.0085	0.038	0.023	ns	ns	ns	

the code ***** is used when the p value is smaller than 0.00001 and ns indicates a not significant result.

thought to not be constant during the test due to inhomogeneity in the abradable.

Mean and maximum force and temperature data have been extracted from the results for each test and are shown in Table 1 as well as the results of XRF analysis for transfer from the blade to the abradable. T tests between these results and the results for other incursion rates are also summarised.

As shown, this incursion rate produced significantly lower mean forces and temperatures than other incursion rates. Blade samples from these tests also show significantly less wear than either of the other incursion rates.

The above results have been analysed for trends with abradable hardness and blade speed. The results of this analysis are shown in Table 1. As shown significant trends for increasing maximum forces and temperature with abradable hardness and lower forces with higher speeds. More blade wear was also significantly correlated with higher abradable hardness.

3.1.2. 0.2 μm/pass

Abradable samples from tests at 0.2 $\mu m/pass$ (example shown in Fig. 6B) had a similar appearance to those tested at 0.02 $\mu m/pass$. However, notably smaller wear tracks and more extensive areas of smeared metal on the surface are observed at 0.2 $\mu/pass$. As above blades (Fig. 6A) show some thermal discolouration and shear lips on the trailing edges. Wear debris (Fig. 6G) again showed particles much larger than the incursion depth made up most of the debris.

Force, temperature and blade length results from these tests (Fig. 6 C and D) show consistent blade wear throughout the test. While forces and temperatures rapidly increase at the start of the test then plateau or reduce slightly as the test progresses.

As above the results from all of these tests have been summarised in Table 2. As shown this incursion rate produces forces and temperatures lower than those observed for tests at 2 $\mu m/pass$ but higher than those from tests at 0.02 $\mu m/pass$. Differences between these incursion rates were significant for forces while mean temperatures were significantly higher than tests at 0.02 $\mu m/pass$. In addition tests at this incursion rate produces significantly more blade wear than the other incursion rates.

Within this incursion rate significant trends for lower forces and higher mean temperature were seen with increasing speed. Trends for higher maximum normal force and more blade wear with increasing abradable hardness were also significant.

3.1.3. 2 μm/pass

Abradable samples from tests at 2 $\mu m/pass$ showed small wear tracks with some areas of transfer and some crater like features consistent with spalling mechanisms as shown in Fig. 7 B. SEM examination of the rubbed surface (Fig. 7B) showed it had become compacted. Blade samples were similar to those described above for other incursion rates however some also show adhesions to the leading face. As above wear debris consisted of particles lager than the 2 μm Incursion depth.

At 2 $\mu m/pass$ collected data, such as those in Fig. 7 C and D, show a sharp increase in force to very high level. This increase in forces precedes the onset of blade wear and a raise in temperature.

Results from all tests with the NiCrAl Bentonite abradable at 2 $\mu m/pass$ are summarised in Table 3. As shown this incursion rate produced significantly higher forces and mean temperatures than either of the other incursion rates. Blade wear was significantly higher than for tests at 0.02 $\mu m/pass$ but significantly lower than measured for tests at 0.2 $\mu m/pass$.

Within the results for this incursion rate a significant trend for higher mean normal force with higher abradable hardness was observed. No other significant trends with either abradable hardness or blade speed were observed.

3.1.4. Compaction analyses

Abradable samples from the tests above at 200 m/s were sectioned and images which allow compaction in the microstructure to be identified were taken. Images are taken with the rubbed surface at the top of the image. The images are segmented by binary threshold [13] to give the metal phase. They are then split into ten strips corresponding to different depths below the rubbed surface. The metal content from these strips is compared to values taken from a control set of images of an abradable which has not been rubbed. The maximum depth at which a significant difference is observed is taken as the depth of compaction.

The results from these analyses are given in Table 4. As shown abradable from the hard batches showed significant compaction at the high incursion rate, these abradables show severe compaction with some large subsurface cracks as shown in Fig. 8A. Further SEM

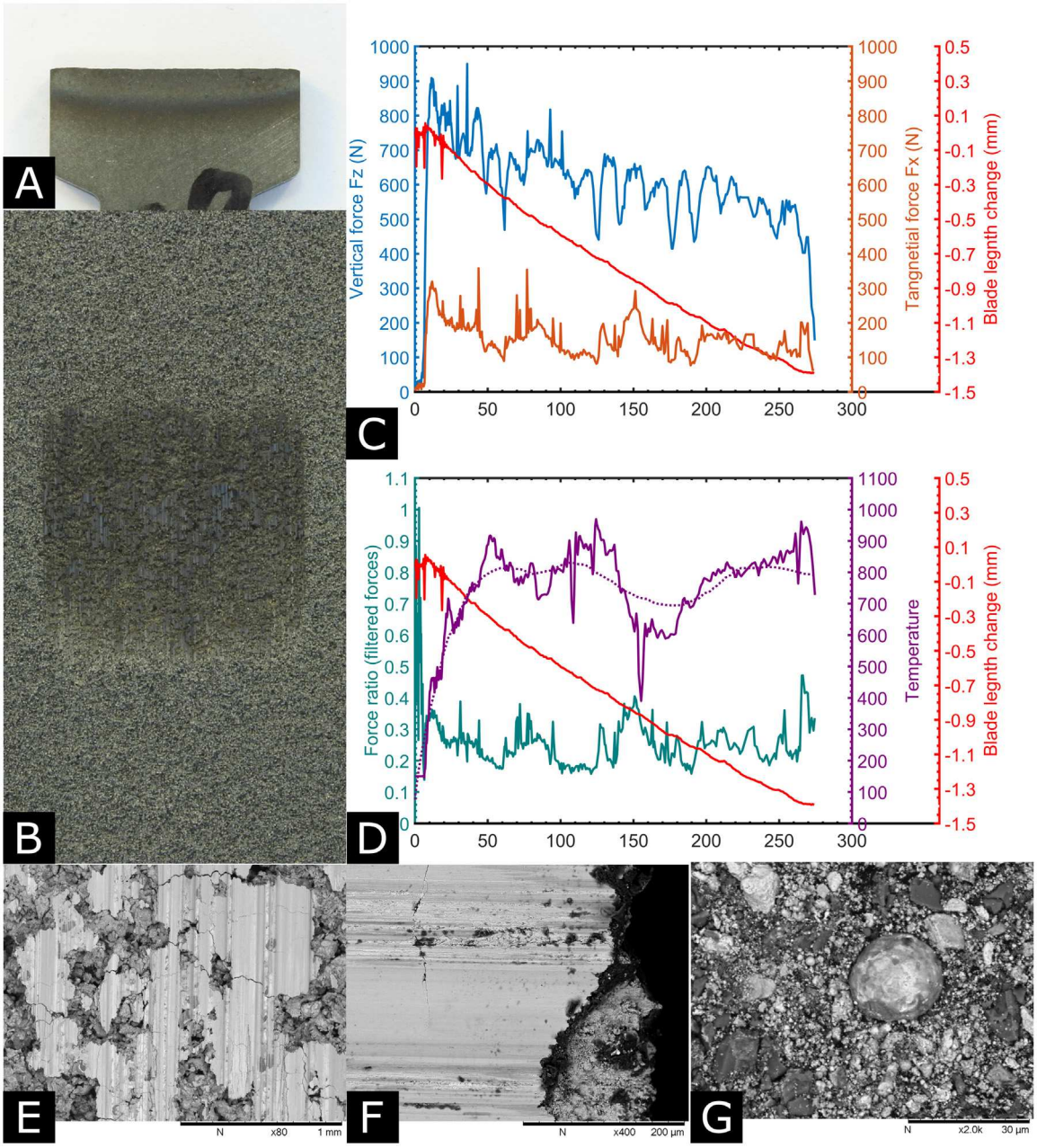

Fig. 6. A–G showing example blade (A) and abradable (B) samples, force and blade length results(C), Temperature and force ratio results (D), and micrographs of the post test abradable surface (E) blade tip (F) and wear debris (G) from tests at 0.2 $\mu m/pass$ against the NiCrAl bentonite abradable.

examination of sections from lower incursion rate tests shows areas of local compaction at the rubbed surface as shown in Fig. 8B. No visible compaction was observed at the surface of the softer abradable.

3.2. AlSi-Polyester vs Ti(6Al 4 V)

As above for the NiCrAl bentonite abradable results for this abradable are presented by incursion rate as this is the most important factor and the main driver of the wear mechanism present as identified by previous works [10]. Again results from each incursion rate are compared to those from the other incursion rates.

3.2.1. 0.02 µm/pass

Tests at the lowest incursion rate against the softer two batches produced grooved wear tracks with groves running parallel to the motion of the blade. These groves corresponded to areas of blade wear and adhesion on to the blade. For the hardest batch the blade was worn across it's entire width. SEM examination and XRF showed areas of transfer of blade material on the abradable surface where blades had worn. This behaviour is as described by Stringer and Marshall [11] for similar incursion rates.

Wear debris for the two softer batches had adhered thickly onto the SEM stub and particles were not distinct indicating they had been at

Table 2
Summary of the test data and statistical tests from tests against the NiCrAl bentonite abradable at 0.2 $\mu m/pass$.

H_a	V_b	I_r	F_n (N)		F_t (N)		T_a $(°C)$		Δ_{bl}	XRF
(HR15Y)	(m/s)	$(\mu m/pass)$	Mean	Max	Mean	Max	Mean	Max	mm	(p)
31	100	0.2	980	2170	460	810	550	850	− 0.79	*****
31	150	0.2	620	1100	350	610	570	820	− 0.60	*****
31	200	0.2	490	900	250	540	600	890	− 0.86	0.00015
50	100	0.2	2160	3270	900	1790	450	900	− 1.2	*****
50	150	0.2	1080	1920	450	720	540	900	− 1.3	*****
50	200	0.2	480	1320	180	330	670	900	− 1.4	*****
54	100	0.2	1720	3280	800	1650	400	800	− 1.2	*****
54	150	0.2	970	2090	390	710	510	860	− 1.1	*****
54	200	0.2	610	980	180	390	680	960	− 1.4	*****
p vs 0.02 $\mu m/pass$			0.0023	0.00084	0.0094	ns	0.00078	ns	0.0011	
p vs 2 $\mu m/pass$			0.018	0.00068	0.00060	0.00085	ns	ns	0.036	
Trend with H_a				+ ve					− ve	
Significance of trend			ns	0.014	ns	ns	ns	ns	0.00091	
Trend with V_b			− ve	− ve	− ve	− ve	+ ve			
Significance of trend			0.0037	0.00031	0.025	0.0069	0.0039	ns	ns	

the code ***** is used when the p value is smaller than 0.00001 and ns indicates a not significant result.

least partly molten when removed, this is shown in Fig. 9 G.

Force and temperature results showed cyclic behaviour similar to that described above for the NiCrAl bentonite vs Inconel 718 rub but with generally lower forces and abradable surface temperature. This is shown in Fig. 9 C and D. Although abradable temperatures are relatively low (310–690 °C) blade temperatures are likely to be much higher, this is supported by bluing of the blade tips, as shown in Fig. 9A. It is thought that in these circumstances the blades wears by

Results from this incursion rate for rubbing forces, abradable temperature and final blade length change are summarised in Table 5. This incursion rate produced the lowest mean forces of any incursion rate tested, and lower rubbing temperatures than the highest incursion rate. There was also significantly more blade wear at this incursion rate than seen for the highest incursion rate. Other differences were not significant.

These results show significant trends for higher tangential forces, higher maximum normal force and more blade wear with higher abradable hardness. No significant trends with blade speed were observed.

3.2.2. 0.2 $\mu m/pass$

At 0.2 $\mu m/pass$ the abradable was generally cleanly cut with some adhesions present on the blade as described by Stringer and Marshall [11], however tests against the hardest batch of abradable produced severe blade wear. At this incursion rate XRF analysis indicates transfer from the blade to the abradable for the highest hardness spray batch. As above wear debris had thickly adhered to the SEM stubs for the softer spray batches.

At this incursion rate for the intermediate and soft batches blade length data show adhesions periodically growing and breaking as previously for AlSi based abradables [10,12,6] shown in Fig. 10 C and D. In addition to this increasing forces and temperatures are seen just before the onset of adhesion on to the blade. Periods of adhesive growth show higher force ratios than the rest of the test.

These data are summarised in Table 6 for all tests at this incursion rate. Comparisons with other incursion rates show that 0.2 $\mu m/pass$ produces intermediate mean forces significantly different from other incursion rates and significantly lower mean temperature, max tangential force and more blade wear than observed for the highest incursion rate.

Within this incursion rate significant trends for higher mean forces, temperatures and more blade wear with higher abradable hardness were observed. No significant trends were observed with blade speed.

3.2.3. 2 $\mu m/pass$

At the highest incursion rate all abradables appeared cleanly cut and all blades showed some small adhesions to the blade tip. At this incursion rate wear debris (Fig. 11G) consisted of distinct particles mostly of diameter $2 - 10\ \mu m$ with some particles up to 50 μm.

Blade length and force data (Fig. 11C) for these tests show gradually increasing blade length indicating adhesions growing through out the test. Forces and temperature increase initially but plateau or reduce as the test progresses.

As above these data are summarised for all testes at this incursion rate in Table 7. Comparisons with other incursion rates are also summarised in Table 7. This incursion rate produced significantly higher mean forces, maximum tangential force and temperature than either other incursion rate. Blade wear was also significantly lower at this incursion rate than either of the lower incursion rates.

At this incursion rate significant trends for higher forces, temperatures and lower final blade length were observed with increasing abradable hardness. Trends for higher temperatures were observed with increasing blade speed.

4. Wear mechanisms

The results above and previous work in this field indicate the wear mechanisms in each rub. These are summarised below for each of the rubs investigated here. In the case of the NiCrAl bentonite abradable the mechanism is not discussed in previous work, thus, a mechanism is suggested.

These mechanisms will be used to generate terms which should, if the wear mechanisms are correct, be related to the measured parameters of: force, blade length change and abradable temperature. The equations are not intended to be a perfect description of the extremely complex rub. Instead they will provide a starting point for fitting a linear model.

This represents the first attempt to provide a predictive model based on wear mechanisms and experimental results. Such a model, if sufficiently accurate, would be invaluable to dynamics models of the

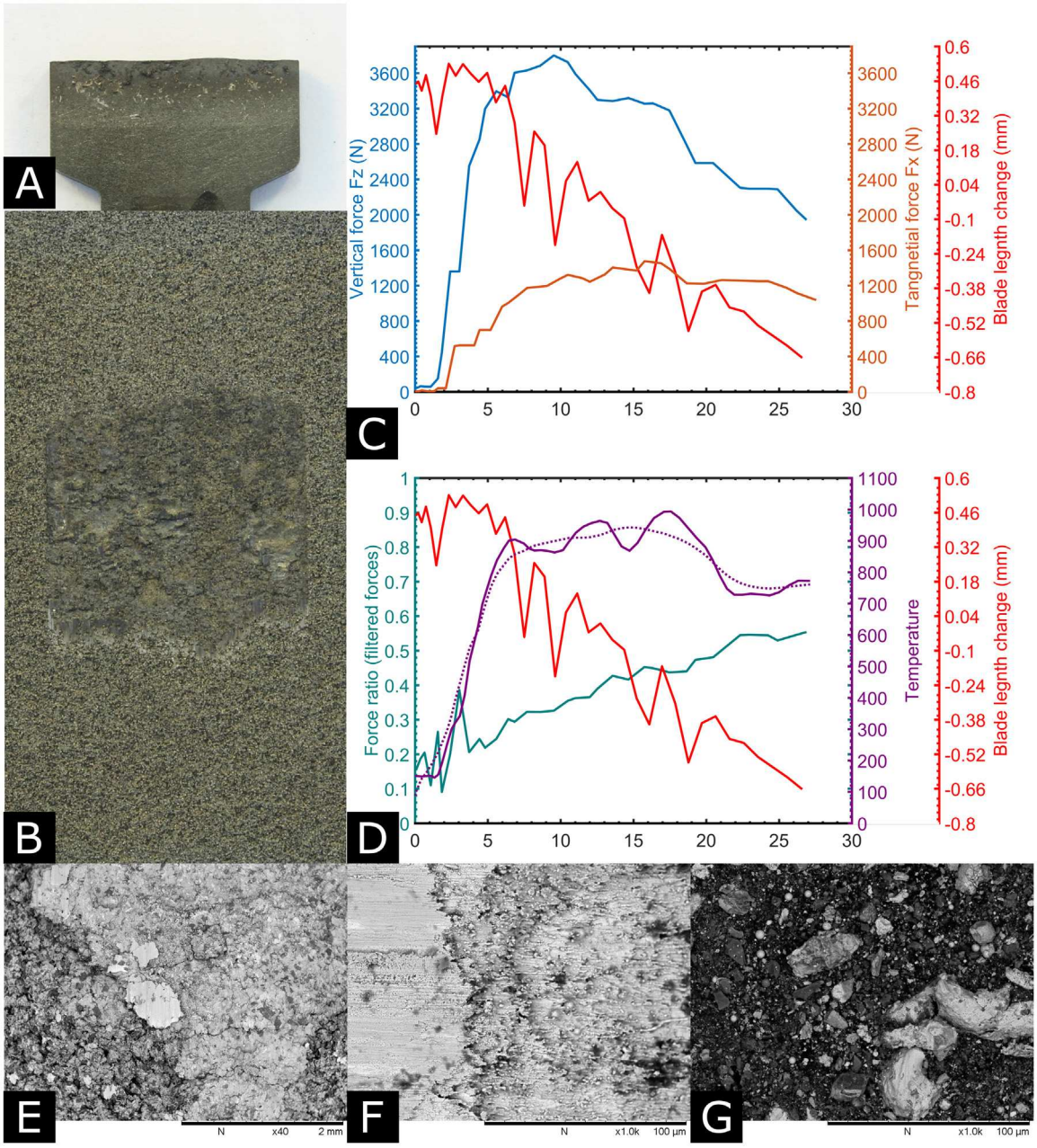

Fig. 7. A–G showing example blade (A) and abradable (B) samples, force and blade length results(C), Temperature and force ratio results (D), and micrographs of the post test abradable surface (E) blade tip (F) and wear debris (G) from tests at 2 $\mu m/pass$ against the NiCrAl bentonite abradable.

compressor system. It would also allow for comparison between spray batches and aid in the development of new abradables.

4.1. NiCrAl-bentonite vs Inconel 718

It is proposed that the repeated impact of the blade leads to sub-surface damage growing cracks witch are already present in the microstructure. This leads to the removal of particles much larger than the incursion depth. The resulting removal rate of abradable from the surface is proportional to the kinetic energy imparted by the blade and the amount or connectivity of cracks already present in the microstructure.

This yields Eq. (1) which describes the mean thickness removed per strike. In which D_a is the thickness removed, H_a is the hardness of the abradable, taken here as a proxy for the amount of cracking in the microstructure, and C_1 is a constant. The V_b^2 term represents the kinetic energy input from the blade.

$$D_a = C_1 H_a V_b^2 \tag{1}$$

The normal force is the force necessary to displace the abradable

Table 3
Summary of the test data and statistical tests from tests against the NiCrAl bentonite abradable at 2 $\mu m/pass$.

H_a	V_b	I_r	F_n (N)		F_t (N)		T_a $(°C)$		Δ_{bl}	XRF
(HR15Y)	(m/s)	$(\mu m/pass)$	Mean	Max	Mean	Max	Mean	Max	mm	(p)
31	100	2	1200	3210	880	2030	570	870	− 0.57	*****
31	150	2	1560	4670	590	1010	530	930	− 0.74	*****
31	200	2	680	1280	600	1150	500	740	− 0.69	0.00074
50	100	2	1780	4400	1340	3380	610	860	− 0.44	*****
50	150	2	2770	5200	900	2140	500	870	− 1.0	*****
50	200	2	1460	3770	550	1190	490	≥ 1000	− 0.79	*****
54	100	2	1840	4420	720	1610	620	860	− 0.57	*****
54	150	2	2880	5110	840	1530	740	≥ 1000	− 1.4	*****
54	200	2	2070	3760	820	1500	680	≥ 1000	− 1.0	*****
p vs 0.02 $\mu m/pass$			0.00043	8.8e− 5	6.6e− 5	0.0013	0.00011	ns	0.048	
p vs 0.2 $\mu m/pass$			0.018	0.00068	0.00060	0.00085	ns	ns	0.036	
Trend with H_a			+ve							
Significance of trend			0.043	ns	ns	ns	ns	ns	ns	
Trend with V_b										
Significance of trend			ns	ns	ns	ns	ns	ns	ns	

the code ***** is used when the p value is smaller than 0.00001 and ns indicates a not significant result.

Table 4
Compaction analysis results from abradable tested at 200 m/s.

Incursion rate	0.02 $\mu m/pass$			0.2 $\mu m/pass$			2 $\mu m/pass$		
HR15Y	50	54	31	50	54	31	50	54	31
Depth (μm)	–	–	–	–	–	–	383	553	–
Significance	ns	ns	ns	ns	ns	ns	*	*	ns

*indicates a significant result at the p < 0.05 level.

under the blade tip with the tangential force simply being this multiplied by the friction coefficient and a factor to take account of the deformation in the abradable. This is given in Eq. (2) in which H_s is the hardness of the abradable surface, $F(I_r)$ is a function of the incursion rate that takes the dynamic effects of the blade impact into account, A_t is the contact area between the blade and the abradable and C_2, C_3 are constants.

$$\begin{aligned} F_n &= C_2 H_s(H_a, D_a, F(I_r)A_t) \\ F_t &= (\mu + C_3)F_n \end{aligned} \quad (2)$$

Lastly the temperature of the surface is given by Eq. (3) Which can be thought of as a term describing the heat into the surface C_4F_t and the ability of the surface to loose heat C_5H_a/V_b in which the hardness of the abradable is taken as a proxy for the thermal diffusivity.

$$T_a = C_4F_t + C_5\frac{H_a}{V_b} \quad (3)$$

If the damage caused to the abradable is not enough to accommodate the incursion parts of the surface become compacted. This increases the stiffness of these parts of the abradable surface. More of the surface also comes into contact with the blade as it is pressed flat. This leads to higher forces and temperatures.

Blade wear occurs when the force needed to shear the blade tip is less than the shear force at the contact. This criterion is summarised in Eq. (4) in which $\tau(T_b)$ is the shear strength of the blade tip as a function of the blade tip's temperature.

$$\tau(T_b) < \sqrt{\frac{F_n}{2A_t}^2 + \frac{F_t}{A_t}^2} \quad (4)$$

The mechanism proposed above provides an explanation to the

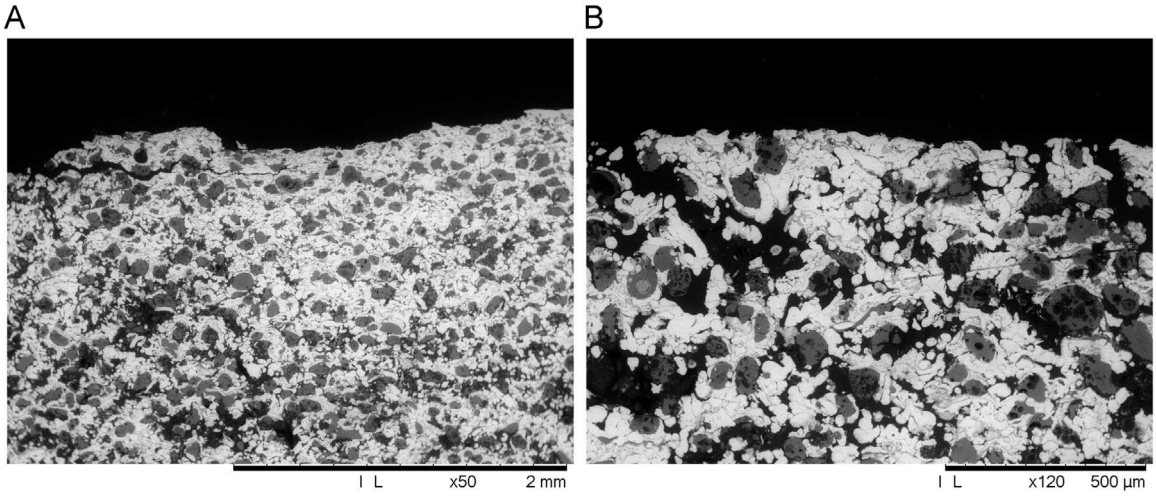

Fig. 8. A and B showing a micrograph of the abradable from tests against batch B at 2 $\mu m/pass$ showing severe compaction and subsurface cracking and a micrograph of an abradable from tests against batch A at 0.02 $\mu m/pass$ showing local compaction at the surface.

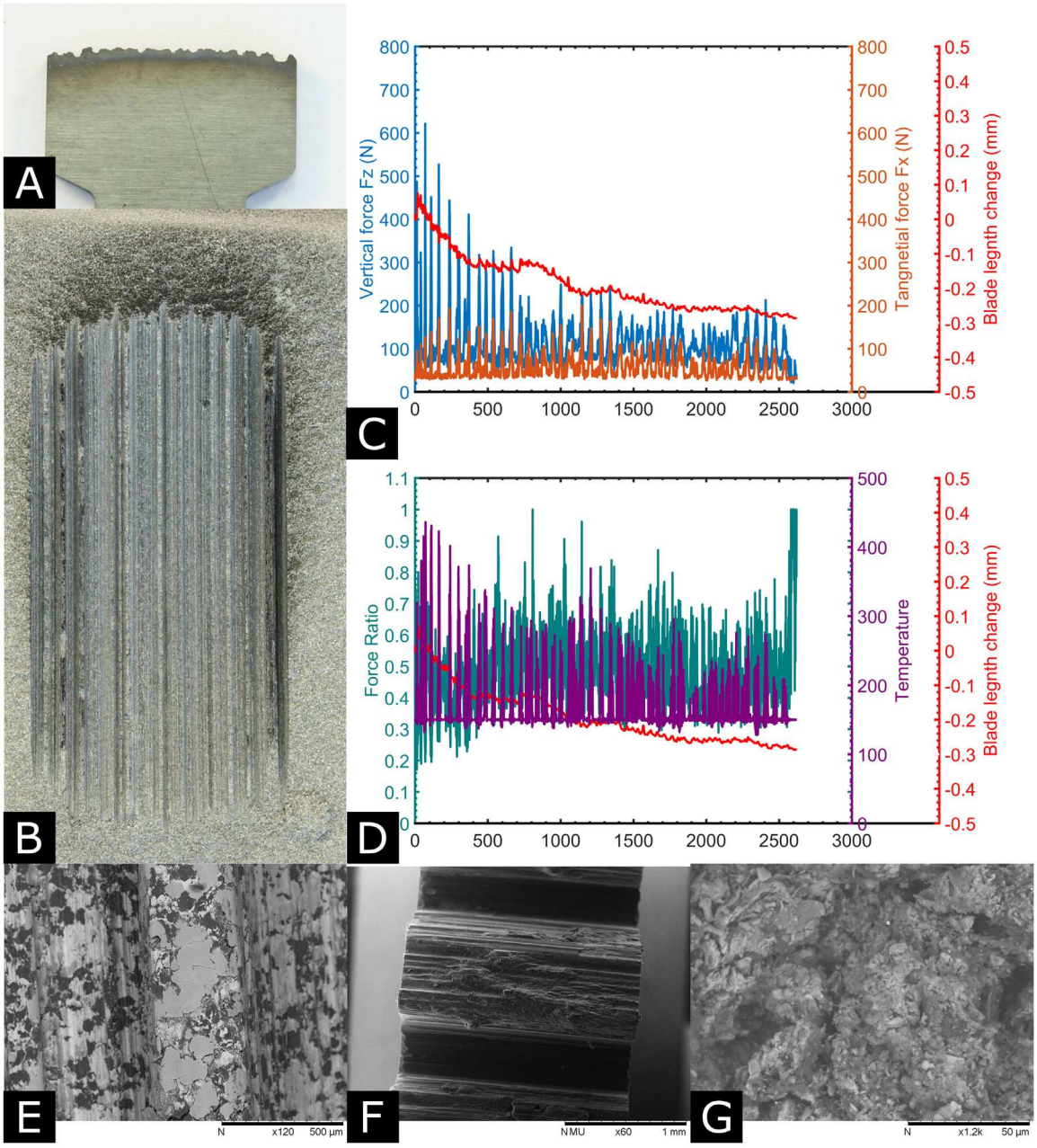

Fig. 9. A–G showing example blade (A) and abradable (B) samples, force and blade length results(C), Temperature and force ratio results (D), and micrographs of the post test abradable surface (E) blade tip (F) and wear debris (G) from tests at 0.02 $\mu m/pass$ against the AlSi polyester abradable.

behaviour seen in the results section. At low incursion rates, for the soft coating, damage to the abradable comes quickly enough to accommodate the incursion of the blade. For the harder abradables some localised compaction, which appears as smeared areas with no porosity at the surface, leads periodically to increasing forces and temperatures until the blade is soft enough to wear. These areas can be removed by further sub surface damage.

At the mid incursion rate, the same mechanism occurs but high blade temperatures are maintained leading to consistent blade wear throughout the test. These tests show increasing forces and temperatures at the start of the test. At the onset of blade wear temperature plateaus but forces are reduced.

At the highest incursion rate, damage to the abradable cannot accommodate the incursion of the blade. Areas are compacted under the blade tip while the blade increases in temperature. When the blade is hot enough to wear, according to Eq. (4), blade wear begins and forces are reduced slightly.

Behaviour seen with lower blade speeds is also explained by this model as the slower blade causes less damage per pass to the abradable leading to higher forces. Additionally trends for lower temperature at lower speeds are explained as there is more time between strikes for heat to move away from the contacting surfaces.

Table 5
Summary of the test data and statistical tests from tests against the AlSi polyester abradable at 0.02 $\mu m/pass$.

H_a	V_b	I_r	F_n (N)		F_t (N)		T_a $(°C)$		Δ_{bl}	XRF
(HR15Y)	(m/s)	$(\mu m/pass)$	Mean	Max	Mean	Max	Mean	Max	mm	(p)
55	100	0.02	70	450	30	180	150	310	0.051	ns
55	150	0.02	100	310	40	180	170	510	− 0.038	ns
55	200	0.02	70	320	30	150	160	690	− 0.013	ns
63	100	0.02	90	490	40	150	160	410	− 0.12	0.024
63	150	0.02	90	570	40	180	170	530	− 0.18	0.00039
63	200	0.02	120	620	60	200	170	440	− 0.30	*****
79	100	0.02	140	970	50	500	160	410	− 0.96	*****
79	150	0.02	140	940	60	590	170	530	− 1.0	*****
79	200	0.02	90	610	40	370	170	510	− 1.0	*****
p vs 0.2 $\mu m/pass$			0.036	ns	0.012	ns	ns	ns	0.086	
p vs 2 $\mu m/pass$			0.0014	ns	0.00057	0.012	0.00030	ns	0.00019	
Trend with H_a				+ve	+ve	+ve			−ve	
Significance of trend			ns	0.00024	0.027	0.0023	ns	ns	*****	
Trend with V_b										
Significance of trend			ns	ns	ns	ns	ns	ns	ns	

the code ***** is used when the p value is smaller than 0.00001 and ns indicates a not significant result.

4.2. AlSi polyester vs Ti(6Al 4 V)

At the low incursion rate the abradable and blade are worn by adhesive and abrasive wear [5,2]. The contact can be described by the Archard equation which is given in Eq. (5). The worn volume per length rubbed can be considered as the incursion rate multiplied by length of the blade in the axial direction. Rearranging Eq. (5) gives an expression for the normal force in the rub. This and the related equation for tangential force are given by Eq. (6) in which C_7 is a constant.

$$V_w = I_r L_a = \frac{C_6 F_n}{H_a} \tag{5}$$

$$\begin{aligned} F_n &= C_7 I_r H_a \\ F_t &= \mu F_n \end{aligned} \tag{6}$$

Under this mechanism the temperature of the rubbing surface can be described in a similar way to the equation given above for the NiCrAl bentonite abradable. This is given in Eq. (7) in which the C_8 and C_9 are constants and the $C_8 F_t$ term can be though of as the heat into the surface where as the $C_9 V_b H_a$ term can be thought of as the ability of the abradable to remove heat from the surface.

$$T_a = C_8 F_t + C_9 V_b H_a \tag{7}$$

The wear on the blade is determined only by the hardness of the abradable as shown in Eq. (8) in which C_{10} is a constant.

$$\Delta_{bl} = C_{10} H_a \tag{8}$$

At the high incursion rate the abradable is worn by cutting in a process analogous to turning. As every blade has the same rake and clearance angles the forces on the blade are determined by the cut depth (incursion rate) and shear strength of the abradable. This is summarised in Eq. (9) in which the hardness of the abradable acts as a proxy measure for it's shear strength and C_{11} and C_{12} are constants.

$$\begin{aligned} F_n &= C_{11} I_r H_a \\ F_t &= C_{12} I_r H_a \end{aligned} \tag{9}$$

The temperature of the abradable surface in these situations is described by the Peclet number which is given in Eq. (10) [6]. With the assumption that the hardness of the abradable can be used as a proxy measure for it's thermal diffusivity this becomes Eq. (11)

$$T_a \propto Pe = \frac{V_b I_r}{\alpha} \tag{10}$$

$$T_a = C_{13} \frac{V_b I_r}{H_a} \tag{11}$$

The wear mechanisms described above have been found by examination of the worn samples, force results and wear debris. They are in line with previous work in the field on similar abradables by this and other groups [2].

5. Statistical modelling

The above mechanisms have been used to generate factors for mechanism based linear models which have been fitted to the results for rubbing forces, abradable temperature and blade length. The factors proposed above for each of these dependent variables have been fitted to the mean values measured during each test. This process gives a method to evaluate the quality of the proposed mechanisms objectively and indicate which processes are best understood and if this approach is relevant to abradable contacts. Models such as these are frequently used to merge analytical understanding and measured data [14].

5.1. Model Description

The function between incursion rate and normal force for the NiCrAl bentonite vs Inconel 718 rub is likely to be extremely complicated due to dynamic effects in the contact occurring at the scale of non-linearities in the abradable microstructure. For the sake of model fitting several simple functions have been tried and the best fitting (log) has been selected. A physical description of the underlying process would be purely speculative and is not given.

The mechanism described above can be mathematically summarised as shown in Eq. (12) below. This model was fitted to the data from the above tests using a linear model with the factors listed in Table 8.

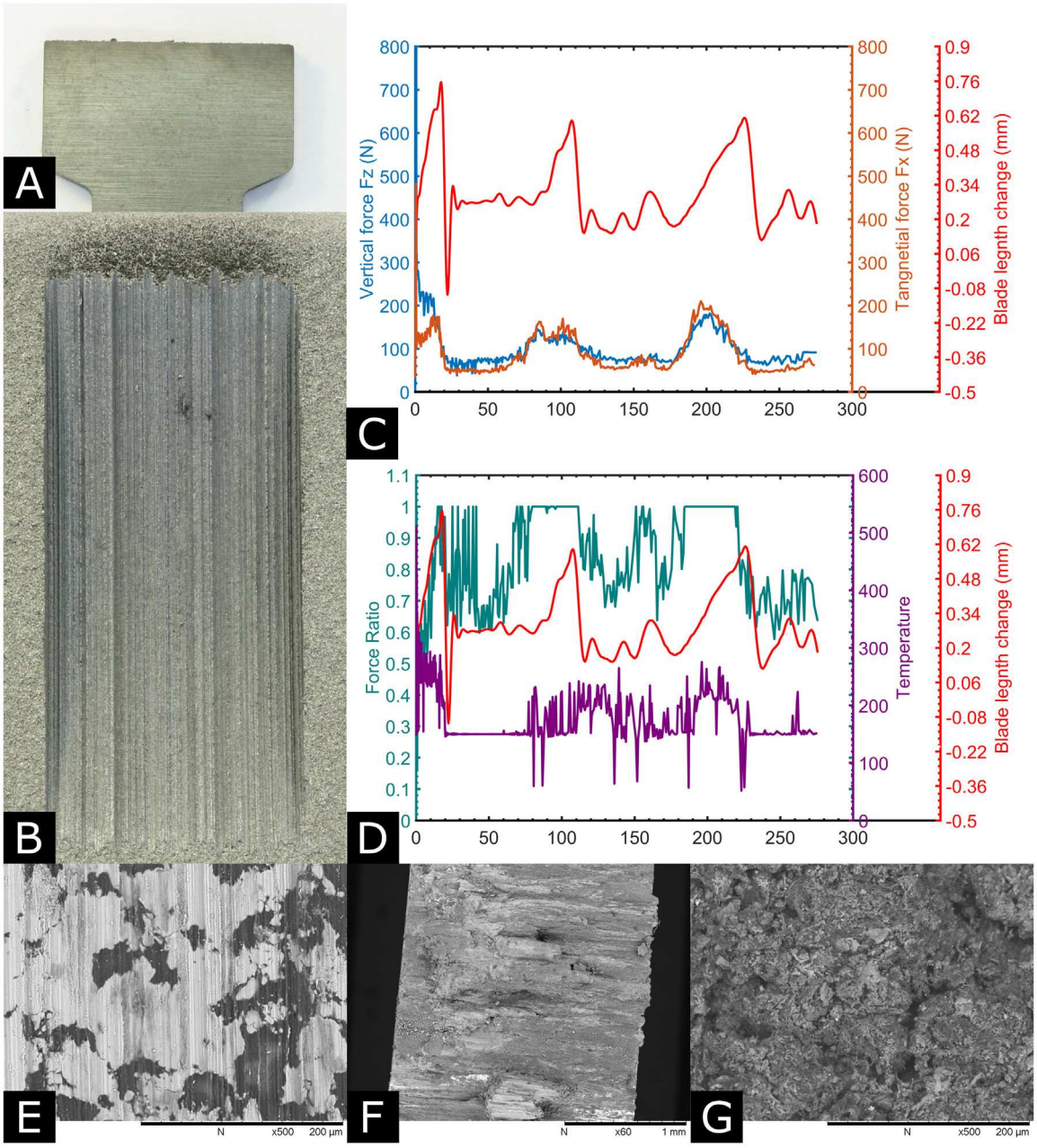

Fig. 10. A–G showing example blade (A) and abradable (B) samples, force and blade length results(C), Temperature and force ratio results (D), and micrographs of the post test abradable surface (E) blade tip (F) and wear debris (G) from tests at 0.2 $\mu m/pass$ against the AlSi polyester abradable.

$$\begin{aligned} F_n &= F_{fn}(log(I_r)H_a,\ H_aV_b^2,\ H_a,\ I_r) \\ F_t &= F_{ft}(log(I_r)H_a,\ H_aV_b^2,\ H_a,\ I_r) \\ T_a &= F_{ta}(log(I_r)H_a,\ H_aV_b,\ I_r) \\ \Delta_{bl} &= F_{bl}(log(I_r)H_a,\ H_aV_b^2,\ H_a,\ I_r) \end{aligned} \tag{12}$$

For the AlSi polyester vs Ti(6Al 4 V) the mechanism has been mathematically summarised in Eq. (13). In order to generalise between the two wear mechanisms present for this rub the terms expected from each are multiplied by the incursion rate. This allows the model to compensate for the change in wear mechanism with incursion rate. As above the relations between the hardness on the HR15Y scale and the thermal diffusivity are not known. For the sake of model fitting several simple functions have been tried and the best performing chosen (cubic).

Table 6
Summary of the test data and statistical tests from tests against the AlSi polyester abradable at 0.2 $\mu m/pass$.

H_a	V_b	I_r	F_n (N)		F_t (N)		T_a $(°C)$		Δ_{bl}	XRF
(HR15Y)	(m/s)	$(\mu m/pass)$	Mean	Max	Mean	Max	Mean	Max	mm	(p)
55	100	0.2	127	431	66	210	154	319	0.115	ns
55	150	0.2	101	234	57	103	156	259	0.008	ns
55	200	0.2	115	226	53	94	166	255	0.025	ns
63	100	0.2	116	402	51	163	145	200	0.076	ns
63	150	0.2	117	262	72	168	153	245	0.018	ns
63	200	0.2	117	1316	94	482	184	510	0.293	ns
79	100	0.2	476	1139	183	403	326	486	− 0.909	*****
79	150	0.2	331	1120	243	620	332	494	− 0.876	*****
79	200	0.2	282	561	117	224	416	538	− 1.156	*****
p vs 0.02 $\mu m/pass$			0.036	ns	0.012	ns	ns	ns	0.086	
p vs 2 $\mu m/pass$			0.00054	ns	0.00017	0.023	0.047	ns	0.0087	
Trend with H_a			+ve		+ve		+ve	+ve	−ve	
Significance of trend			0.0024	ns	0.0082	0.00075	0.016	0.0021	ns	
Trend with V_b										
Significance of trend			ns	ns	ns	ns	ns	ns	ns	

the code ***** is used when the p value is smaller than 0.00001 and ns indicates a non significant result.

$$\begin{aligned} F_n &= F_{fn}(I_r H_a,\ I_r,\ I_r^2 H_a) \\ F_t &= F_{ft}(I_r H_a,\ I_r,\ I_r^2 H_a) \\ T_a &= F_{ta}(I_r H_a,\ I_r,\ I_r^2 H_a,\ V_b I_r / H_a^3) \\ \Delta_{bl} &= F_{bl}(H_a I_r,\ I_r) \end{aligned} \tag{13}$$

5.2. Model performance

The above equations have been used to inform fitting a general linear model (GLM) for each of the measured variables discussed above. Where factors were non significant they were removed to reduce the complexity of the model. The results of this procedure are shown in Table 8 for the NiCrAl bentonite vs Inconel 718 rub and Table 9 for the AlSi polyester vs Ti(6Al 4 V) rub.

Plots of predicted vs measured values for each of the variables fitted are shown in Fig. 12 for the NiCrAl bentonite vs Inconel 718 rub and Fig. 13 for the AlSi polyester vs Ti(6Al 4 V) rub. As shown forces and, to some extent, blade length change correlate well with this model however the temperature of the abradable does not.

Q-Q plots of the residuals are shown in Figs. 14 and 15. These results show the residuals (difference between predicted and measured value) are relatively normally distributed (Lie on the line X = Y) for force estimates with the exception of tangential force in the AlSi polyester vs Ti(6Al 4 V) rub. The residuals for temperature and blade length data are also not normally distributed indicating that either the system is not linear or factors have been missed in the formulation of these models.

6. Discussion

High speed wear tests have been completed on several spray batches of two separate abradables in order to show differences between the wear mechanisms present. A large volume of tests were completed allowing trends within the results to be statistically tested for the first time in abradables research. Mechanisms were suggested that would intuitively fit these trends.

It is suggested that the NiCrAl bentonite abradable wears in each case by compression under the blade leading to sub surface damage to the microstructure. While it is suggested that the AlSi polyester abradable wears by adhesive/ abrasive mechanisms at low incursion rates but is cut at high incursion rates as previously seen by others [5,2]. These mechanisms are distinct and conflict in important ways. It is unlikely that there will exist a single contact model that will work in all abradable contacts. The concise descriptions of these mechanisms allows clear hypotheses to be generated which will be tested in future works in order to validate the proposed mechanisms.

Linear models of the mean results and final blade length change were generated from mathematical descriptions of these wear mechanisms. These were strongly correlated with the measured values for rubbing forces ($R^2 = 0.926 - 0.963$). This suggests that the mathematical descriptions of the rubbing forces and the mechanisms that provide the foundation to these are accurate, with the exception of the tangential forces for the AlSi polyester vs Ti (6Al, 4 V) rub.

Abradable temperature and blade length change were less well correlated, non normally distributed residuals shown in QQ plots above indicate that the sources of this error are either non linearities or missed effects in the system. There are many potential sources of non-linearity in the thermal system including the effects of different test lengths. In addition blade length change is not expected to be linear due to growing and breaking of adhesions to the blade tip.

Implicit in these models is an assumption that the mean result is representative of the test as a whole. For force results from tests with intermediate and high incursion rates this is a reasonable assumption, however at lower incursion rates periodic behaviour is observed for both abradables and temperature results from very short tests are transient. However despite this limitation, the models in their current state still provide an essential method for comparing potential new technologies to a range of typical behaviour.

These limitations could be resolved through the use of more sophisticated transient models which could be trained on time coded data from entire tests. Due to the intermittent nature of some of the phenomena presented above this may be the only method to model or predict rubbing temperatures to a reasonable accuracy. Such models

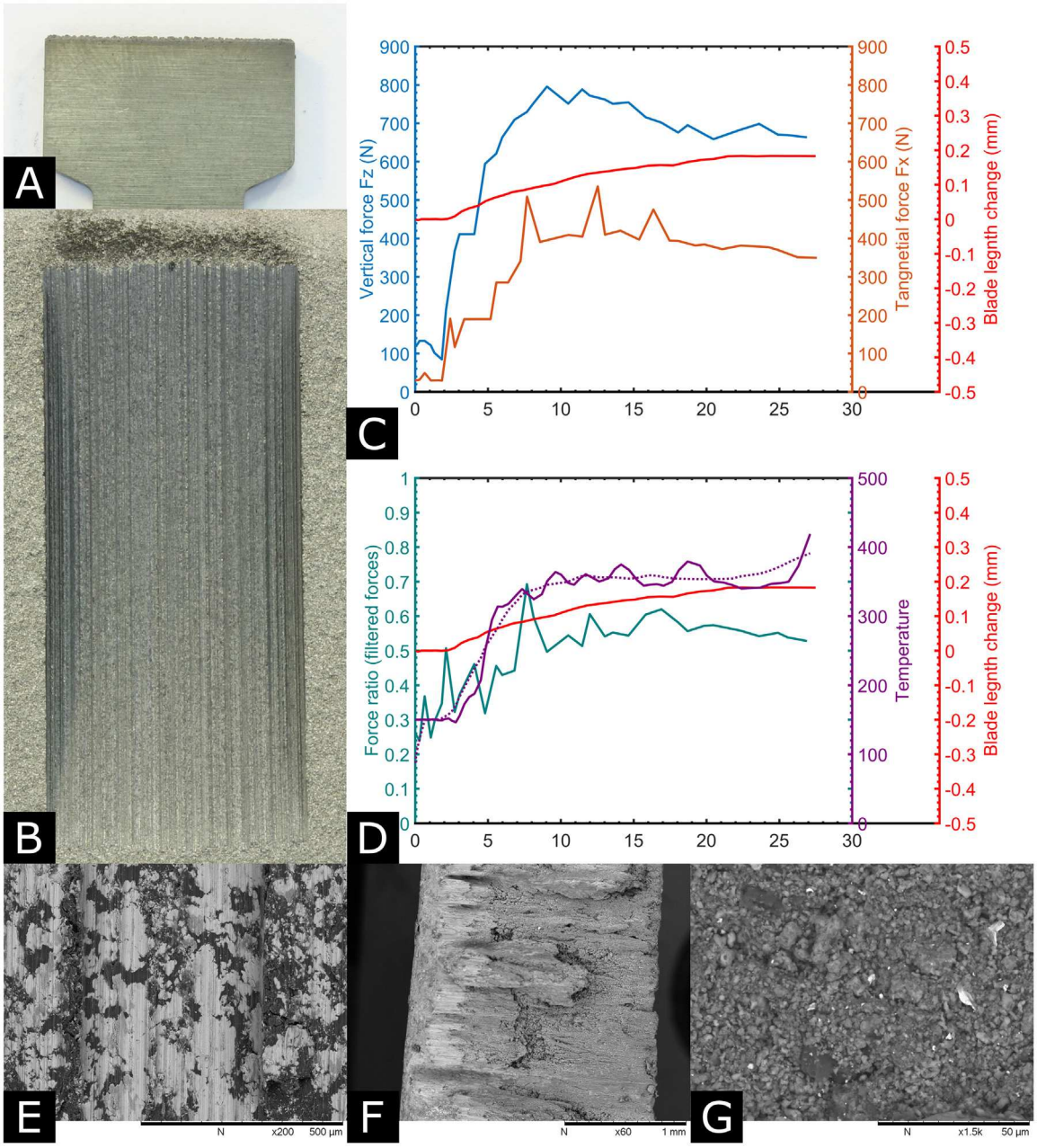

Fig. 11. A–G showing example blade (A) and abradable (B) samples, force and blade length results(C), Temperature and force ratio results (D), and micrographs of the post test abradable surface (E) blade tip (F) and wear debris (G) from tests at 2 $\mu m/pass$ against the AlSi polyester abradable.

Table 7
Summary of the test data and statistical tests from tests against the AlSi polyester abradable at 2 $\mu m/pass$.

H_a	V_b	I_r	F_n (N)		F_t (N)		T_a $(°C)$		Δ_{bl}	XRF
(HR15Y)	(m/s)	$(\mu m/pass)$	Mean	Max	Mean	Max	Mean	Max	mm	(p)
55	100	2	300	570	180	370	220	260	0.58	ns
55	150	2	300	760	190	350	240	330	0.49	ns
55	200	2	370	520	210	330	270	370	0.24	ns
63	100	2	350	760	220	400	220	280	0.16	ns
63	150	2	420	600	270	390	230	330	0.25	ns
63	200	2	560	800	300	540	290	420	0.18	ns
79	100	2	1020	1350	560	910	290	480	− 0.28	*****
79	150	2	1020	3170	620	1159	290	530	− 0.038	*****
79	200	2	1020	3980	420	1730	400	610	− 0.040	ns
p vs 0.02 $\mu m/pass$			0.0014	ns	0.00057	0.012	0.00030	ns	0.00019	
p vs 0.2 $\mu m/pass$			0.00054	ns	0.00017	0.023	0.047	ns	0.0087	
Trend with H_a			+ve	+ve	+ve	+ve	+ve	+ve	−ve	
Significance of trend			2.5e− 5	0.075	0.00069	0.0020	0.0057	6.7e− 5	0.0023	
Trend with V_b							+ve	+ve		
Significance of trend			ns	ns	ns	ns	0.013	0.0024	ns	

the code ***** is used when the p value is smaller than 0.00001 and ns indicates a non significant result.

Table 8
Results of the GLM fitting for the output variables in the NiCrAl Bentonite vs Inconel 718 rub.

Variable	F_n		F_t		T_a		Δ_{bl}	
R^2	0.932		0.928		0.542		0.907	
Adj. R^2	0.924		0.920		0.504		0.891	
p-value	3.6e− 14		6.8e− 14		8.4e− 5		1.6e− 11	
	Coef.	p	Coef.	p	Coef.	p	Coef.	p
Intercept	–	–	–	–	466	4.0e− 8	–	–
$log(I_r)H_a$	6.95	8.4e− 9	2.79	6.19e− 8	1.16	2.7e− 5	− 0.00414	0.0048
$H_aV_b^2$	− 4.21e− 4	0.0023	− 2.39e− 4	2.5e− 4	–	–	1.22e− 6	3.3e− 4
H_a	45.1	4.7e− 12	20.7	3.1e− 12	–	–	–	–
V_bH_a	–	–	–	–	0.0155	0.071	–3.96e− 4	6.2e− 6
I_r	–	–	–	–	–	–	0.332	0.015

Table 9
Results of the GLM fitting for the output variables in the AlSi polyester vs Ti(6Al 4 V) rub.

Variable	F_n		F_t		T_a		Δ_{bl}	
R^2	0.963		0.959		0.750		0.878	
Adj. R^2	0.958		0.954		0.690		0.868	
p-value	<2.2e − 16		<2.2e − 16		9.9e− 6		1.1e− 11	
	Coef.	p	Coef.	p	Coef.	p	Coef.	p
Intercept	–	–	–	–	152	8.9e− 9	2.29	4.8e− 10
I_r	− 706	8.2e− 8	− 326	2.4e− 6	− 262	0.016	–	–
H_a	–	–	–	–	–	–	− 0.041	2.1e− 11
I_rH_a	28.5	2.0e− 10	14.1	2.8e− 9	17.3	2.7e− 6	4.3e− 3	1.1e− 7
$I_r^2H_a$	− 6.60	8.9e− 6	− 3.32	4.4e− 5	− 6.61	2.6e− 5	–	–
V_bI_r/H_a^3	–	–	–	–	− 7.41e5	0.0031	–	–
$V_bI_r^2/H_a^3$	–	–	–	–	4.15e5	0.0012	–	–

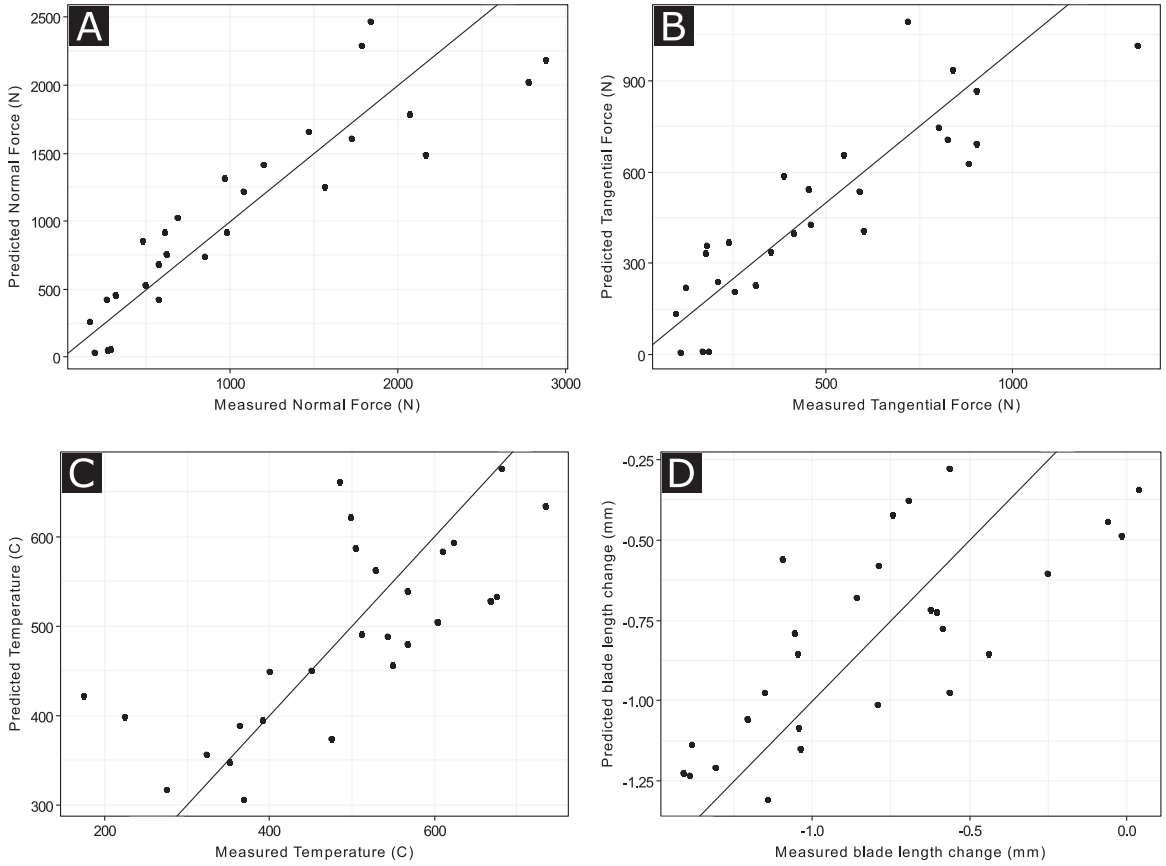

Fig. 12. A–D showing predicted vs measured values for the models produced above for mean normal force (A) mean tangential force (B) mean abradable temperature (C) and blade length change (D).

could be used to predict rubbing behaviour for a given spray batch, optimise the specification range or intended incursion conditions of in service abradables more rigorously than the current norm. More complex rubbing conditions, such as variable incursion rates, as seen in service, could also be investigated with a drastic reduction in the number of tests needed.

7. Conclusions

For both of the abradables tested harder batches of abradable produced more blade wear and higher normal forces, for the AlSi polyester abradable higher tangential forces and abradable temperatures were also seen. Substantial differences between batches were observed and it clear that future work in this field should not focus on single spray batches as if they are representative of all batches as found previously for the AlSi hBN abradable [6].

Blade speed was shown to be an important factor for the NiCrAl bentonite rub, with higher speeds resulting in lower forces, higher temperatures and less blade wear. Blade speed was not an important factor in the AlSi polyester vs Ti rub over the range tested ($100 - 200\ m/s$).

These results show that the knowledge of the wear mechanisms present in these rubs is sufficient to model them statistically, with accurate models possible for rubbing forces. Further modelling research from this group will focus on transient models which can be applied to full data sets and models of rubbing temperatures which are essential for understanding blade wear.

A substantial limitation of this study is that the maximum blade speed is half that used in service. The force measurement system is also only capable of measuring indicative forces. If this process were repeated on a fully representative test rig with a sophisticated force measurement system such as the Ohio State university rig [15] a rubbing force model of great worth to compressor dynamics studies could be generated.

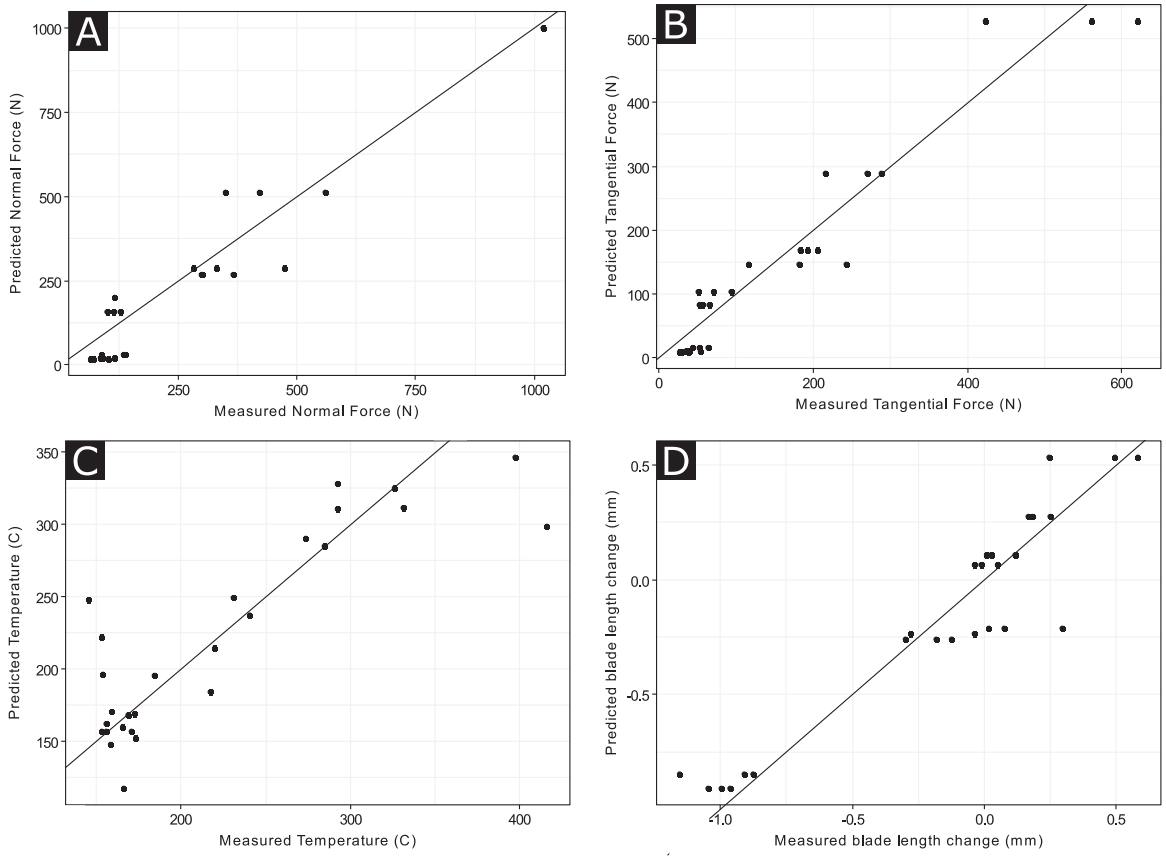

Fig. 13. A–D showing predicted vs measured values for the models produced above for mean normal force (A) mean tangential force (B) mean abradable temperature (C) and blade length change (D).

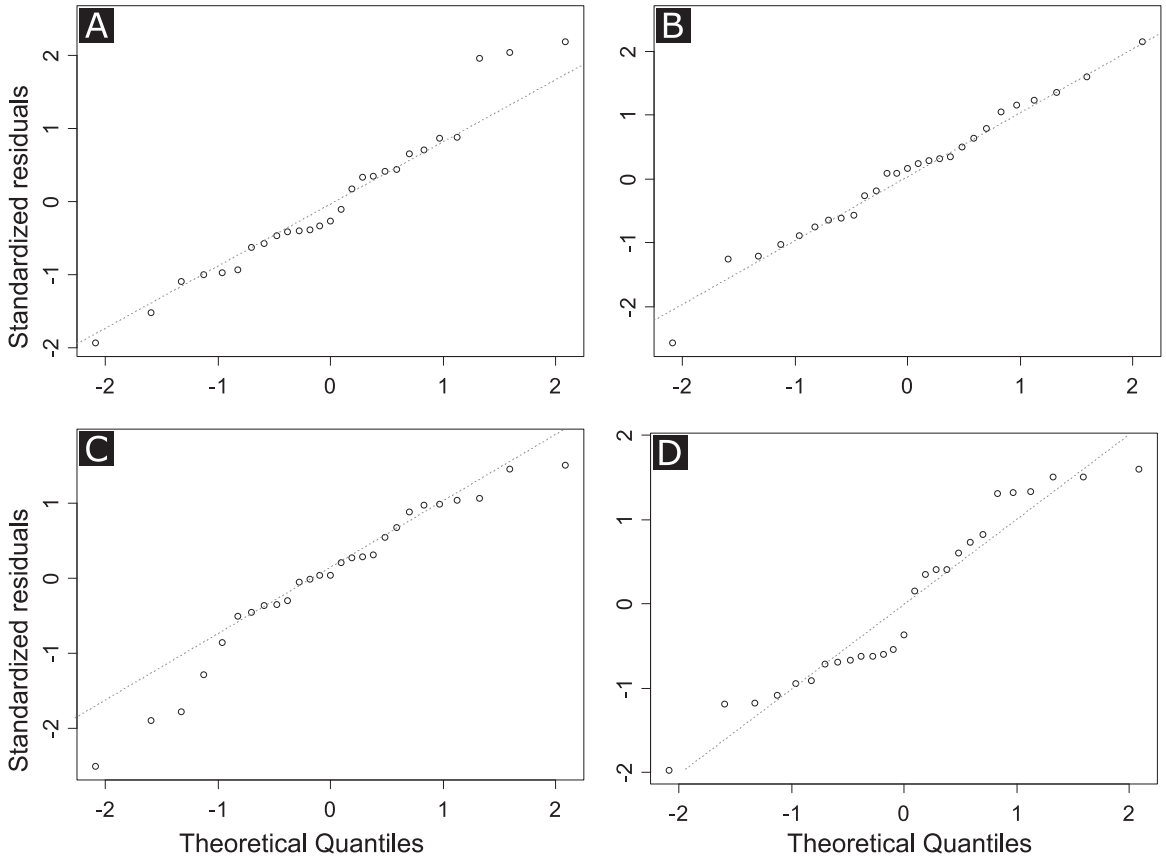

Fig. 14. A–D showing Q–Q plot of the residuals for the models produced above for mean normal force (A) mean tangential force (B) mean abradable temperature (C) and blade length change (D) for the NiCrAl bentonite vs Inconel 718 rub.

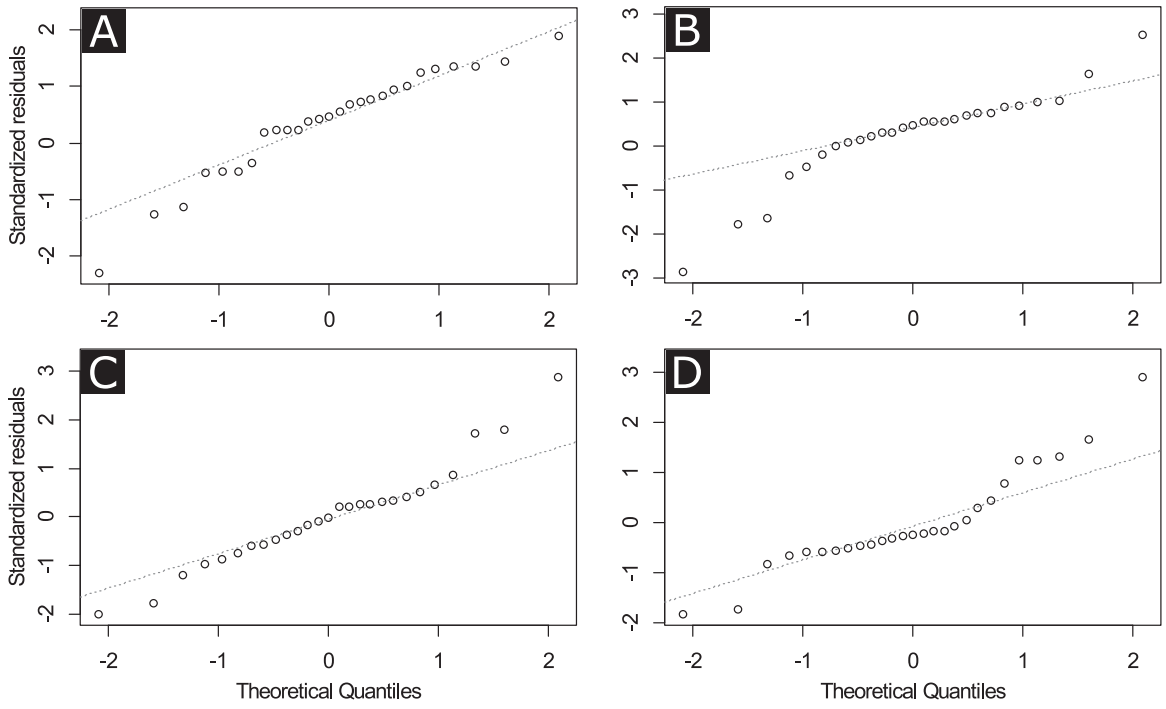

Fig. 15. A–D showing Q–Q plot of the residuals for the models produced above for mean normal force (A) mean tangential force (B) mean abradable temperature (C) and blade length change (D) for the AlSi polyester vs Ti(6Al 4 V) rub.

Funding

This work was funded by the EPSRC (Award No. EP/H023895/1) and Rolls Royce plc.

References

[1] R. Chupp, F. Ghasripoor, G. Moore, Applying Abradable Seals to Industrial Gas Turbines, in: Proceedings of the 38th AIAA/ASME/SAE/ASEE Joint Propulsion Conference & Exhibit, Joint Propulsion Conferences, American Institute of Aeronautics and Astronautics, 2002. URL ⟨http://dx.doi.org/10.2514/6.2002-3795⟩.

[2] D. Sporer, S. Wilson, S.M. Ag, current and next-generation titanium blade compatible compressor abradable coatings, in: Proceedings from the International Thermal Spray Conference And Exposition, 2012, pp. 143–148.

[3] Sultzer Metco, Material Product Data Sheet Aluminum Silicon Hexag-onal Boron Nitride Abradable. (2014), 1–3.

[4] Sultzer Metco, Material Product Data Sheet Nickel Chromium Alu-minum / Bentonite Abradable Powders (2012). URL ⟨http://www.oerlikon.com/ecomaXL/files/oerlikon_TS_MaterialGuide_EN_052012.pdf⟩.

[5] M. Borel, A. Nicoll, R. Schmid, The wear mechanisms occurring in abradable seals of gas turbines, Surf. Coat. Technol. 40 (1989) 117–126 (URL ⟨http://www.sciencedirect.com/science/article/pii/0257897289900467 ⟩).

[6] N. Fois, M. Watson, M. Marshall, The influence of material properties on the wear of abradable materials, institution of mechanical engineers, Proc. Part J. Eng. Tribol. 0 (0) (2016) 1–14, http://dx.doi.org/10.1177/1350650116649528 (URL ⟨http://pij.sagepub.com/lookup/doi/10.1177/1350650116649528 ⟩).

[7] M. Watson, M. Marshall, A. Novel Image, Segmentation approach for microstructure modelling, Coatings 7 (10) (2017) 166, http://dx.doi.org/10.3390/coatings7100166 (URL ⟨http://www.mdpi.com/2079-6412/7/10/166 ⟩).

[8] T. Taylor, B. Thompson, W. Aton, High speed rub wear mechanism in IN-718 vs NiCrAlBentonite, Surf. Coat. Technol. 202 (4–7) (2007) 698–703, http://dx.doi.org/10.1016/j.surfcoat.2007.05.054 (URL ⟨http://linkinghub.elsevier.com/retrieve/pii/S025789720700549X ⟩).

[9] M. Watson, N. Fois, M.B. Marshall, Effects of blade surface treatments in tip shroud abradable contacts, Wear 338–339 (2015) 268–281, http://dx.doi.org/10.1016/j.wear.2015.06.018 (URL ⟨http://dx.doi.org/10.1016/j.wear.2015.06.018⟩).

[10] N. Fois, J. Stringer, M. Marshall, Adhesive transfer in aero-engine abradable linings contact, Wear 304 (1–2) (2013) 202–210, http://dx.doi.org/10.1016/j.wear.2013.04.033 (URL ⟨http://linkinghub.elsevier.com/retrieve/pii/S0043164813002755 ⟩).

[11] J. Stringer, M. Marshall, High speed wear testing of an abradable coating, Wear 294–295 (2012) 257–263, http://dx.doi.org/10.1016/j.wear.2012.07.009 (URL ⟨http://linkinghub.elsevier.com/retrieve/pii/S0043164812002529 ⟩).

[12] N. Fois, M. Watson, J. Stringer, M. Marshall, An investigation of the relationship between wear and contact force for abradable materials, in: Proceedings of the Institution of Mechanical Engineers, Part J: Journal of Engineering Tribology http://dx.doi.org/10.1177/1350650114545139. URL ⟨http://pij.sagepub.com/lookup/doi/10.1177/1350650114545139⟩.

[13] N. Otsu, A threshold selection method from gray-level histograms, Autom. C 1 (1975) 62–66 (URL ⟨http://web-ext.u-aizu.ac.jp/course/bmclass/documents/otsu1979.pdf ⟩).

[14] C.M. Bishop, Pattern Recognition and Machine Learning, Springer, Cambridge, 2006 (URL ⟨http://users.isr.ist.utl.pt/wurmd/Livros/school/Bishop-PatternRecognitionAndMachineLearning-Springer2006.pdf ⟩).

[15] C. Padova, J. Barton, M.G. Dunn, S. Manwaring, G. Young, M. Adams, M. Adams, Development of an experimental capability to produce controlled blade tip/shroud rubs at engine speed, J. Turbomach. 127 (4) (2005) 726, http://dx.doi.org/10.1115/1.1934429 (URL ⟨http://turbomachinery.asmedigitalcollection.asme.org/article.aspx?articleid=1467095 ⟩).